 DOI: 10.1002/eji.201344313 Eur. J. Immunol. 2014. 44: 2306–2317

European Journal of Immunology

Static and dynamic components synergize to form a stable survival niche for bone marrow plasma cells

Sandra Zehentmeier[1], Katrin Roth[1], Zoltan Cseresnyes[1], Özen Sercan[1], Katharina Horn[1], Raluca A. Niesner[1], Hyun-Dong Chang[1], Andreas Radbruch[1] and Anja E. Hauser*[1,2]*

[1] Deutsches Rheuma-Forschungszentrum (DRFZ), Institute of the Leibniz-Gemeinschaft, Berlin, Germany
[2] Charité Universitätsmedizin, Berlin, Germany

In the bone marrow (BM), memory plasma cells (PCs) survive for long time periods in dedicated microenvironmental survival niches, resting in terms of proliferation. Several cell types, such as eosinophils and reticular stromal cells, have been reported to contribute to the survival niche of memory PCs. However, until now it has not been demonstrated whether the niche is formed by a fixed cellular microenvironment. By intravital microscopy, we provide for the first time evidence that the direct contacts formed between PCs and reticular stromal cells are stable in vivo, and thus the PCs are sessile in their niches. The majority (~80%) of PCs directly contact reticular stromal cells in a non-random fashion. The mesenchymal reticular stromal cells in contact with memory PCs are not proliferating. On the other hand, we show here that eosinophils in the vicinity of long-lived PCs are vigorously proliferating cells and represent a dynamic component of the survival niche. In contrast, if eosinophils are depleted by irradiation, newly generated eosinophils localize in the vicinity of radiation-resistant PCs and the stromal cells. These results suggest that memory PC niches may provide attraction for eosinophils to maintain stability with fluctuating yet essential accessory cells.

Keywords: Bone marrow · Intravital microscopy · Plasma cells · Stromal cells · Survival niche


See accompanying Commentary by Tellier and Kallies


Additional supporting information may be found in the online version of this article at the publisher's web-site

Introduction

The prominent role of the bone marrow (BM) for the maintenance of resting immunological memory is becoming increasingly evident. Several types of memory lymphocytes have been identified which are maintained predominantly in the BM [1]. Long-lived, resting memory plasma cells (PCs) reside in the BM [2] and resting professional memory $CD4^+$ T cells have been located to the BM as well [3]. The BM is thought to sustain the survival of these different memory immune cell populations in cell-specific microanatomical niches [4, 5]. PCs have been shown to depend on extrinsic survival factors to survive and their colocalization with several cell types which produce these survival factors has been demonstrated by histology. They are in close contact with reticular stromal cells producing chemokine (CXC motif) ligand 12 (CXCL12) [6], a chemokine which has been shown to regulate PC immigration into the BM [7, 8], but which also acts as a potent PC survival factor in vitro [9]. Blocking of leukocyte

Correspondence: Prof. Anja E. Hauser
e-mail: hauser@drfz.de

*These authors contributed equally to this work.

function-associated antigen 1 (LFA-1) and very late antigen 4 (VLA-4) purges PCs from their BM niches [10], indicating a role for these adhesion molecules in the interaction between PCs and stromal cells. Interleukin 6 (IL-6) has been shown to support PC survival in vivo [11]. Another crucial component of the survival niche is a proliferation-inducing ligand (APRIL) [12, 13], which promotes PC longevity by inducing the antiapoptotic protein myeloid cell leukemia 1 (Mcl1) [14]. In line with this, APRIL- and IL-6-secreting eosinophils are localized in the vicinity of 60% of BM PCs [15]. Genetic deficiency of eosinophils resulted in the depletion of about 70% of long-lived BM PCs in vivo, suggesting that for these PCs, the eosinophils had provided essential survival signals [15]. Eosinophils are generated in the BM, but they are not considered to be long-term residents of bone, as they leave this organ upon maturity [16]. In addition, other hematopoietic cell types such as megakaryocytes [11], dendritic cells [17], basophils [18], and monocytes/macrophages [19] have been reported to contribute to PC maintenance in vivo by provision of survival factors. This raises the basic question whether the stable survival niche for memory PCs indeed contains essential, fluctuating accessory cells, or whether these hematopoietic accessory cells in the PC niches are also nonproliferating, long-lived cells. Here, we show that static components (i.e. PCs and stromal cells) define the survival niche, while accessory eosinophils are a dynamic component.

Results

Plasma cells colocalize with stromal cells in the bone marrow

PCs of the BM have been described to contact reticular stromal cells, but this has not been quantified so far, because of the difficulty to identify contacts between PCs and dendritic extensions of stromal cells. Here we used genetic staining of stromal cells to better visualize their ramifications and potential contacts to PCs. We irradiated C57BL/6 mice expressing either green or red fluorescent protein (GFP or RFP) in all cells, eliminating most hematopoietic cells of the BM. These mice were reconstituted with BM cells of wild type C57BL/6 donors (Supporting Information Fig. 1). While more than 95% of the $CD45^+$ GFP^+ hematopoietic cells of the host were depleted by irradiation, endothelial cells, reticular stromal cells, osteoblasts, and osteocytes expressing GFP were maintained (Fig. 1A and Supporting Information Fig. 2). Reticular stromal cells were $CD45^-$ GFP^+ with long, dendritic extensions that stained positive for vascular cell adhesion molecule 1 (VCAM-1/ CD106), laminin, collagen IV, and fibronectin but neither for the endothelial marker endoglin (CD105) nor the osteoblast marker osteocalcin (Supporting Information Fig. 2). The chimeric mice with nonfluorescent hematopoietic cells were immunized 4 weeks after BM transfer with 4-hydroxy-3-nitrophenylacetyl-coupled chicken gamma globulin (NP-CGG) in Alum, and boosted 21 days later without adjuvant. Thirty days after the last immunization, the BM was analyzed for contacts between PCs (identified by intracellular κ/λ light chain staining), stromal cells and several hematopoietic cell types using a customized, automated image analysis system for two-dimensional confocal images (Fig. 1B). Eleven percent (median, range 4–16%) of the PCs were in direct contact with eosinophils (major basic protein, MBP^+), 7% (2–15%) with megakaryocytes ($CD41^+$), 21% (10–27%) with B cells ($B220^+$), 4% (1–9%) with $CD3^+CD4^-$ T cells, and 2% (0–4%) with other PCs (Fig. 1C). Seventy nine percent (50–81%) of the PCs were in direct, detectable contact with stromal cells (GFP^+) and nearly all (97%, range 74–99%) PCs were in close proximity to stromal cells, i.e. within a distance of 10 μm. Eosinophils were close to 31% (25–46%), megakaryocytes close to 23% (14–36%), B cells close to 52% (37–68%), $CD3^+CD4^-$ T cells close to 18% (9–26%), $CD3^+CD4^+$ T cells close to 6% (2–10%) and other PCs close to 7% (2–22%) of PCs. This analysis underlines the dominance of stroma among the analyzed cell types contacting PCs in the BM.

Plasmablasts are migrating from secondary lymphoid organs to the BM [8]. The high motility of plasmablasts in secondary lymphoid organs has been confirmed by intravital microscopy [20]. However, after arriving in the BM, they loose their in vitro migratory capacity in response to ligands of CXCR3 or CXCR4 [7]. We were interested in whether BM PCs are still motile at all. Intravital microscopy of the tibial BM of mice with GFP^+ stroma and adoptively transferred plasmablasts stained with CellTracker Orange revealed that BM PCs are sessile (Supporting Information Movie 1), at least for the time of observation, i.e. 30 min, and stay in close contact with stromal cells (Fig. 1D and Supporting Information Movie 1 and 2).

To determine whether the direct contacts and the neighborhood of PCs in the BM could be the result of random colocalization, we performed a computer simulation. From individual confocal images of BM (Fig. 1B and C), the area covered by stromal components was used as a matrix on which B cells, eosinophils, and PCs, or megakaryocytes and PCs were repositioned at random. Finally, direct contacts and neighboring cells were analyzed. The frequencies of direct contacts between PCs and stromal cells were about 20% higher in the real confocal images than in the simulations (Fig. 1E and Supporting Information Fig. 5A). This argues that the direct contacts between stromal cells and PCs are not stochastic. Rather, colocalization of these cells is most likely mediated by CXCL12 in order to form a niche for memory PCs, as discussed elsewhere [5]. The frequencies of eosinophils neighboring PCs (10 μm vicinity) were on average 8% higher in confocal images than those in the simulations (Fig. 1E and Supporting Information Fig. 5F). The frequencies of PCs neighboring megakaryocytes were not significantly different between recorded and random images (Fig. 1E and Supporting Information Fig. 5G), thus not supporting a specific localization of megakaryocytes in the niches. PCs neighboring B cells were on average 13% lower in frequency in the confocal images compared with random images (Fig. 1E and Supporting Information Fig. 5H), suggesting that B cells are excluded from PC niches. These results led us to further focus on the dynamics of eosinophils, PCs, and stromal cells forming a niche.

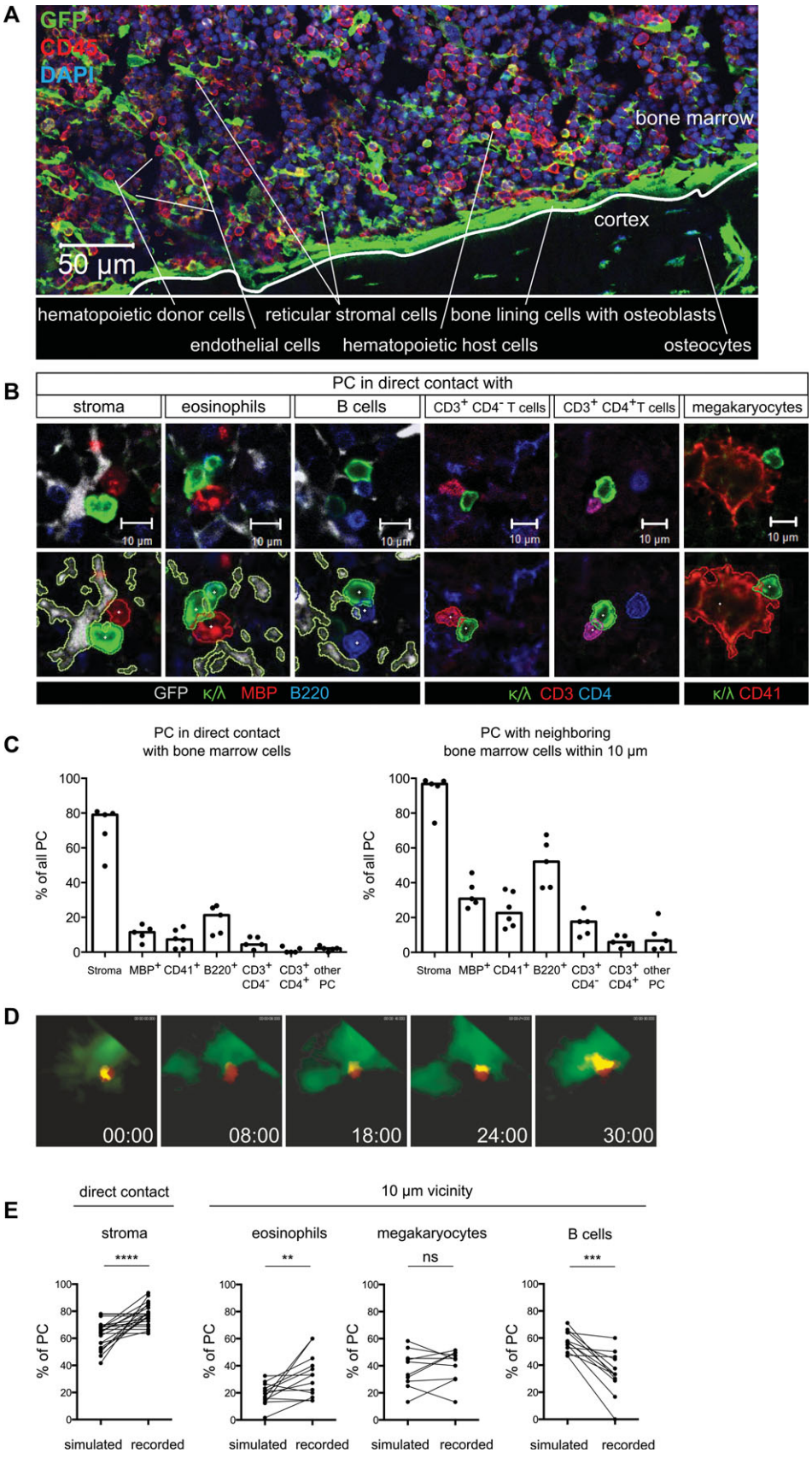

Figure 1. Plasma cells colocalize with stromal cells in the bone marrow (BM). (A) Confocal microscopy of Ubq:GFP/C57BL/6 chimeric femoral BM after staining for CD45 and DAPI. (B) Automated contact and vicinity analysis of BM PCs with various BM cell types on day 30 after boost. Longitudinal BM sections of fluorescent chimeras were stained as indicated and confocal images were analyzed automatically as described in the *Materials and methods*. (C) Quantification of direct contact counts and vicinity analysis of PCs with other BM cells. Data are shown from 52–515 PCs from five to six mice, pooled from two to three independent experiments. Bars indicate median, dots indicate individual mice. (D) Example of a PC (red) forming prolonged contact with BM stroma (green) in vivo, the contact area is shown in yellow. Stills were taken from Supporting Information Movie 2 at indicated time points, a zoom of a 34 × 34 µm area from a projection of seven z-sections is shown. Supporting Information Movie 2 is representative of two mice from independent movie recordings. (E) PC contact and vicinity counts (10 µm distance) in recorded and simulated images. Left: Frequency of PCs in direct contact with stroma (****$p < 0.0001$). Middle: Frequency of PCs in the vicinity of eosinophils (**$p = 0.0081$) or megakaryocytes ($p = 0.5566$). Right: Frequency of PCs in the vicinity of B cells (***$p = 0.0005$). Lines connect recorded images with their corresponding simulated images. Wilcoxon signed rank test, two-sided. Recorded data shown are pooled from two to three independent experiments; 10–21 images per mouse were analyzed. Images from one mouse are displayed for each cell type; five to six mice were analyzed in total. Differences were significant in all five mice for contact frequencies of PCs with stromal cells (Supporting Information Fig. 5A). Significant differences for % of PCs with neighboring eosinophils were found in three of five mice (Supporting Information Fig. 5F). No significant differences for % of PCs with neighboring megakaryocytes were found in five of six mice tested (Supporting Information Fig. 5G). Significant differences for % of PCs with neighboring B cells existed in four of five mice (Supporting Information Fig. 5H).

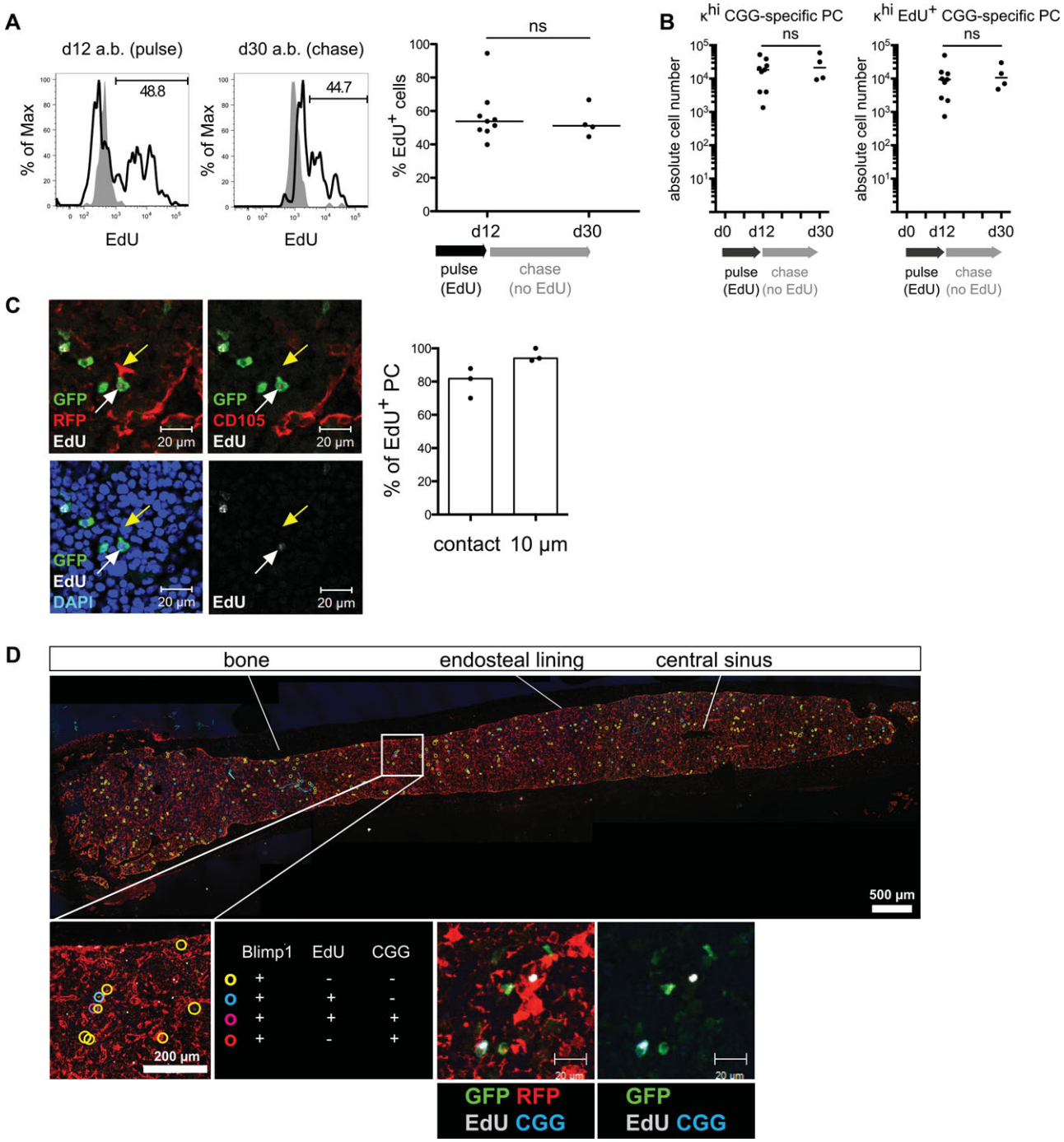

Figure 2. Interaction between long-lived PCs and reticular stromal cells. (A) EdU pulse-chase experiment to detect long-lived PCs in the BM of tdRFP/Blimp-1:GFP chimeric mice. Left: Analysis of EdU labeling of CGG-specific BM PCs by FACS. EdU staining of CGG-specific κ^{hi} BM PCs on day 12 and day 30. Black lines represent $\kappa^{hi}CGG^+$ cells of EdU-fed mice, solid gray areas represent $\kappa^{hi}CGG^+$ cells in immunized controls. Representative histograms of two (day 12, $n = 9$) and one (day 30, $n = 4$) experiments. Full gating strategy provided in Supporting Information Fig. 7. Right: Frequency of EdU^+ cells among $\kappa^{hi}CGG^+$ BM cells on day 12 and day 30. Lines indicate median. Mann–Whitney test, two-sided, $p = 0.7524$. (B) Absolute numbers of CGG-specific κ^{hi} BM PCs as determined in (A). Left: Absolute numbers of CGG-specific κ^{hi} BM PCs on day 12 and day 30 after the second boost. Right: Absolute numbers of CGG-specific $\kappa^{hi}EdU^+$ BM PCs on day 12 and day 30 after the second boost. Mann–Whitney test, two-sided, $p = 0.0642$ (left) and $p = 0.7105$ (right). Lines indicate median. (C) On day 30, EdU^+ PCs directly contact $CD105^-RFP^+$ reticular stromal cells in the BM parenchyma. Manual contact and vicinity analysis of Blimp-1^+EdU^+ PCs on day 30 after the second boost from confocal images of tdRFP/Blimp-1:GFP chimeric BM stained as indicated in the left panel. Yellow arrows mark reticular stromal cells, white arrows mark Blimp-1^+EdU^+ PCs. Bars in the right panel indicate median. Data shown are from three mice, pooled from two independent experiments with 33–55 EdU^+ PCs analyzed per mouse. (D) CGG-specific EdU^+ PCs are equally distributed among the femoral BM. Confocal microscopy of a section of a tdRFP/Blimp-1:GFP chimeric femur on day 30 after the boost stained for GFP, RFP, CGG-Ig, and EdU. Blimp-1^+ PCs are marked with colored circles as indicated. A representative picture of one out of three mice from one experiment is shown.

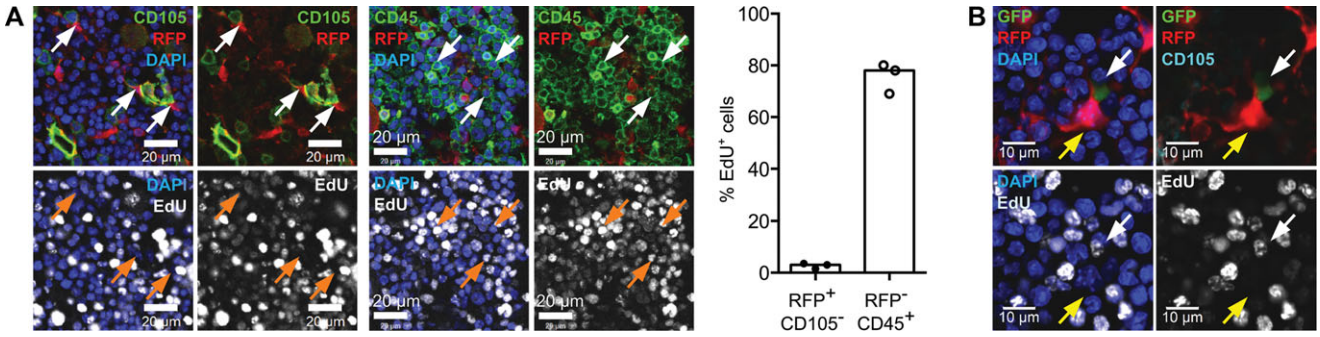

Figure 3. Reticular stromal cells in plasma cell survival niches do not proliferate. (A) Detection of EdU$^+$ stromal nuclei in the BM. Left and middle panel: BM sections of EdU-pulsed tdRFP/Blimp-1:GFP mice on day 12 after boost immunization were stained as indicated and analyzed by confocal microscopy. Arrows mark analyzed nuclei. Right panel: Frequency of EdU$^+$ cells among CD105$^-$RFP$^+$ reticular stromal cells and CD45$^+$RFP$^-$ hematopoietic BM cells determined by manual counting of 200 cells. Bars indicate median. Data shown are pooled from two independent experiments, with one and two individual mice, respectively, and one femoral section per mouse. (B) Analysis of reticular stromal cells in direct contact with long-lived BM PCs. BM sections of EdU-pulsed tdRFP/Blimp-1:GFP mice on day 12 after boost immunization stained were as indicated and analyzed by confocal microscopy. The white arrow marks the nucleus of a Blimp-1$^+$EdU$^+$ PC. The yellow arrow marks the nucleus of a RFP$^+$ reticular stromal cell in direct contact with the marked PC. A representative picture of sections from one out of three mice analyzed in two independent experiments; 31, 12, and 12 PC—stromal cell pairs per mouse were analyzed.

Stability of memory plasma cell niches

It has been demonstrated that memory PCs can survive for extended time periods of at least several months in murine BM [2], and the stability of protective serum antibody titers suggests that they may even survive for decades in man [21]. Here, we analyzed the stability of the survival niche for memory PCs in vivo, with respect to proliferation of the cells and their motility. Proliferation was addressed by in vivo pulse-chase labeling of proliferating cells with the thymidine analogue 5-ethynyl-2′-deoxyuridine (EdU). Chimeric mice with red fluorescent stromal cells, nonfluorescent hematopoietic cells and green PCs were generated by lethal irradiation of tdRFP recipients and adoptive transfer of Blimp-1:GFP BM cells. Four weeks after transfer, the mice were immunized three times with NP-CGG. The mice were fed with EdU for 12 days, following the last immunization (Supporting Information Fig. 6). At the end of the EdU feeding period, 54% (median, range 40–95%) of the CGG-specific κ^{hi} PCs in the BM were EdU$^+$. On day 30 after boost, after a chase period of another 18 days, 51% (45–67%) of the CGG-specific PCs were still EdU$^+$. This indicates that between day 12 and day 30 after immunization, the vast majority of PCs generated in that immune response did not show a high proliferative activity (Fig. 2A and Supporting Information Fig. 7). The numbers of CGG-specific BM PCs remained at a constant level between day 12 and day 30 after immunization (Fig. 2B and Supporting Information Fig. 3A), confirming previous reports in a similar immunization setting [7, 22]. Notably, these numbers did not differ between chimeras and nonirradiated mice (Supporting Information Fig. 3A), indicating that this effect was not due to an altered T-dependent response in the chimeric mice. In the BM, 82% (70–88%) of the newly generated EdU$^+$ PCs directly contacted reticular stromal cells and 94% (93–100%) located in less than 10 μm distance (day 30) (Fig. 2C). They were dispersed evenly all over the BM (Fig. 2D).

In the same experiment reticular stromal cells of the BM were analyzed for proliferation. After the EdU pulse covering the first 12 days following immunization, only 3% (2–4%) of the RFP$^+$CD105$^-$ stromal cells of the BM had taken up EdU (Fig. 3A). In particular, all of the reticular stromal cells directly contacting EdU$^+$ PCs, or localizing within a 10 μm range, were EdU$^-$ (Fig. 3B) and therefore nonproliferative.

In contrast to the resting PCs and stromal cells, eosinophilic granulocytes proliferated strongly. After the EdU pulse, 99% (87–100%) of eosinophils (CD11b$^+$Siglec-F$^+$) had incorporated EdU (Fig. 4A). In particular, also 90% (90–95%) of the eosinophils (MBP$^+$) located in 20 μm vicinity of PCs were EdU$^+$, indicating that eosinophils of the PC niche were as proliferative as all other eosinophils. They maintained their proliferation throughout the chase period of 18 days: On day 30, all of the eosinophils in the PC vicinity had lost their EdU label (Fig. 4B).

Proliferation of eosinophils within and outside of the memory PC niches was confirmed by analysis of BM from mAG-hGeminin mice, which report cells in the S/G_2/M phases of the cell cycle by nuclear green fluorescence [23]. Between 21 and 25% of the eosinophils displayed green nuclei, both of eosinophils in the vicinity of or distant from PCs (Fig. 4C). Taken together both lines of evidence, the EdU pulse-chase labeling and the reporter system, show that eosinophilic granulocytes of the PC survival niches of BM strongly proliferate and comprise a dynamic, fluctuating component of the niche.

Eosinophils repopulate plasma cell survival niches after irradiation

Accessory cells of the BM PC niche provide essential survival signals for PCs [11, 13, 15], but, as we show here for eosinophils, these cells show a high proliferative turnover. In order to maintain a PC over long time periods, the niche has to secure the presence of accessory cells. We tested this by analyzing the repopulation of PC niches with accessory cells after irradiation. For this purpose, we immunized tdRFP mice twice with NP-CGG, fed them with EdU

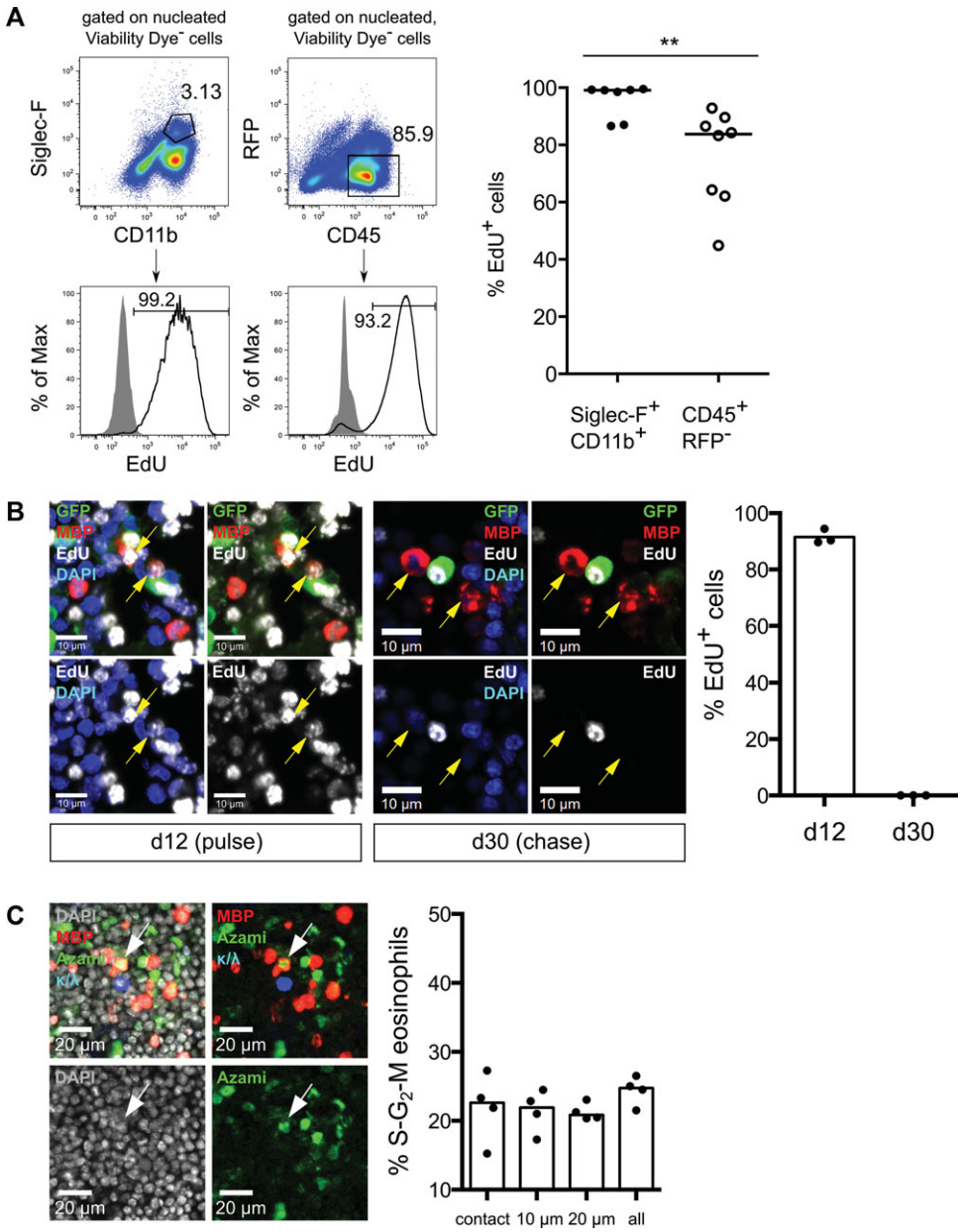

Figure 4. Eosinophils proliferate in the plasma cell niche. (A) EdU-pulse to study the proliferation of BM cells in tdRFP/Blimp-1:GFP chimeras. Left: Frequency of EdU$^+$ cells among Siglec-F$^+$CD11b$^+$ eosinophils and CD45$^+$RFP$^-$ BM cells on day 12 after boost. Black lines in histograms represent eosinophils or CD45$^+$RFP$^-$ cells of EdU-fed mice, solid gray areas represent eosinophils or CD45$^+$RFP$^-$ cells in an immunized control mouse. Right: Frequencies of EdU$^+$ cells among Siglec-F$^+$CD11b$^+$ and CD45$^+$RFP$^-$ BM cells. Data shown are representative of one experiment (eosinophils) or pooled from three independent experiments (CD45$^+$RFP$^-$ cells), with $n = 7$ and $n = 8$ mice total. Lines indicate median. $^{**}p = 0.0037$; Mann–Whitney test, two-sided. Cytometry data was pregated for nucleated, living cells as shown in Supporting Information Fig. 7. (B) Detection of EdU in BM eosinophils in the vicinity of long-lived BM PCs. Confocal microscopy of BM sections on day 12 and day 30 after second boost immunization stained as indicated. Yellow arrows mark the nuclei of eosinophils in the vicinity of EdU$^+$ PCs. Graph depicts the frequency of EdU$^+$ cells among eosinophils neighboring EdU$^+$ PCs within a vicinity of 20 µm on day 12 vs. day 30. Data shown are pooled from two independent experiments, with one and two individual mice, respectively. Sixty to 215 eosinophils counted manually in one femoral section per animal were analyzed. Bars indicate median. (C) Proliferation analysis of niche eosinophils by confocal microscopy of BM sections of CAG-mAG-huGeminin cell cycle reporter mice on day 30 after the first boost. Femoral BM sections of CAG-mAG-huGeminin mice were stained as indicated and analyzed for expression of AzamiGreen in eosinophils. A representative picture of one out of four mice from one experiment is shown. Graph depicts the frequency of S-G2-M (AzamiGreen$^+$) eosinophils in contact with BM PCs or in 10/20 µm vicinity of BM PCs compared with the frequency among all eosinophils. Bars indicate median.

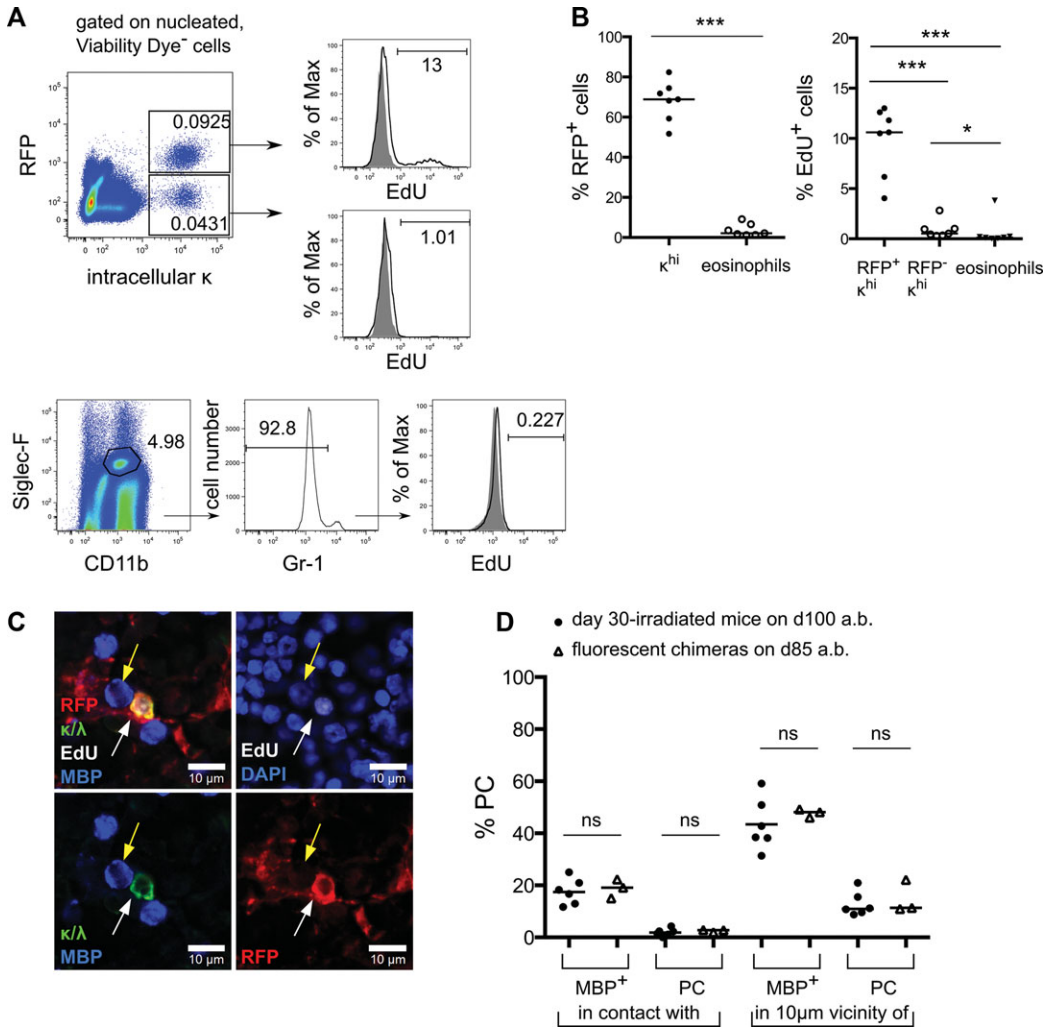

Figure 5. After irradiation accessory cells repopulate the niches where sessile plasma cells and stroma cells persist. (A) FACS analysis of BM PCs and eosinophils in tdRFP mice treated as described in Supporting Information Fig. 9. Upper panel: Frequency of EdU$^+$ cells among κ^{hi}RFP$^-$ (donor) PCs and κ^{hi} RFP$^+$ (recipient) PCs. Black lines in histograms represent PCs of EdU-fed mice, solid gray areas represent PCs in an immunized control mouse. Lower panel: Frequency of EdU$^+$ cells amongst CD11b$^+$Gr-1^{int}Siglec-F$^+$ BM cells. Black lines in histograms represent eosinophils stained for EdU, solid gray areas represent eosinophils in an immunized control mouse. Cytometry data was pregated for nucleated, living cells as shown in Supporting Information Fig. 7. Data shown are representative of one experiment. (B) Frequencies of EdU$^+$ cells amongst PCs and eosinophils as determined in (A) and Supporting Information Fig. 9B. Left panel: % of RFP$^+$ (recipient) cells among κ^{hi} PC and eosinophil populations. Mann–Whitney test, two-sided, $^{***}p = 0.0006$. Lines indicate median. Data collected from one experiment with $n = 7$ mice. Right panel: EdU$^+$ cells amongst recipient PCs, donor PCs and eosinophils as determined in (A). Mann–Whitney test, two-sided (recipient PCs vs. donor PCs: $^{***}p = 0.0006$; donor PCs vs. eosinophils: $^{*}p = 0.0262$; recipient PCs vs. eosinophils: $^{***}p = 0.0006$). Lines indicate median. (C) Confocal microscopy of irradiated tdRFP mice. Femoral BM sections were stained as indicated. The white arrow marks a recipient PC, the yellow arrow a donor eosinophil. A representative picture from one experiment performed with $n = 5$ mice. (D) Automated contact and vicinity analysis (10 µm distance) of PCs and eosinophils in irradiated tdRFP mice on day 100 after the boost and normal fluorescent chimeric mice on day 85 after the boost. No significant differences were found in the % of PCs in contact with eosinophils / other PCs or with neighboring eosinophils / other PCs (10 µm). Mann–Whitney test, two-sided (contact to MBP$^+$ cells: $p = 0.7134$; contact to PCs: $p = 0.381$; neighboring MBP$^+$ cells: $p = 0.5476$; neighboring PCs: $p = 0.381$). Data shown are from one femoral section with 9 to 15 images analyzed per mouse ($n = 6$ and $n = 3$, one experiment per group).

for 12 days after the second immunization and irradiated them on day 30 after the boost (Supporting Information Fig. 9A). Twenty four hours later, we reconstituted the mice with C57BL/6 BM cells. Another 69 days later, on day 100 after the boost, the majority of PCs in the BM was RFP$^+$ (median 69%, range 52–82%), i.e. of host origin. Eleven percent (4–13%) of RFP$^+$ PCs were EdU$^+$, they had been generated in the boost response and had survived the irradiation (Fig. 5A and B). More than 95% of BM eosinophils were donor-derived (RFP$^-$) and EdU$^-$ (Fig. 5A and B, Supporting Information Fig. 9B). Histologically, at this time point, 41% (31–59%) of PCs were in the vicinity of eosinophils (Fig. 5C and D). This is comparable to PCs at day 30 in wild-type mice (Supporting Information Fig. 3) and also to mice analyzed 85 days after a secondary immune reaction (median 48%, range 46–49%) (Fig. 5D). Thus, after irradiation-induced depletion, eosinophils are able to repopulate PC niches, implying a specific mechanism of attraction.

Discussion

Multiple molecular signals derived from different cellular sources are needed to sustain PC survival in the BM niche. In order to understand the complex interplay of these constituents, it is crucial to investigate the PC survival niches in situ. Although much progress has been made recently in identifying the molecular signals involved in PC survival, there are still only few in vivo data on the analysis of PCs in their genuine environment available. Here, for the first time, we analyzed the motility of PCs in the BM using intravital microscopy. We found the majority of these PCs to be sessile, which is in contrast to published data on plasmablasts in secondary lymphoid organs [20] as well as to data on BM B cells [24, 25], which have been shown to be highly motile. Our findings support the concept of stable, fixed survival niches as a prerequisite for the homeostasis of long-lived PCs and extend our earlier findings, which reported a loss of migratory responsiveness toward CXCL12 in long-lived BM PCs [7].

Reticular stromal cells, which are prominent producers of CXCL12 [6, 26], have been previously shown to colocalize with PCs in the BM. We show that PCs actually undergo tight contacts with reticular stromal cells, underlining the importance of this stromal subset for formation and organization of the PC survival niche. The fact that these contacts are nonrandom, as demonstrated by comparison of recorded and simulated images, further underlines the importance of a stroma-based fixation of PCs. We also show that reticular stromal cells form a static component of the PC survival niche not only in terms of motility but also in terms of proliferation. In contrast, we found that eosinophils, which have previously been shown to contribute to the PC niche by providing PC survival factors such as APRIL and IL-6 [15] are a short-lived population. Under certain conditions such as infections, eosinophils which are generally considered to be short-lived, have been shown to exhibit an extended lifetime in peripheral tissues [16], raising the possibility that in PC niches, eosinophils might be long-lived. However, our finding that eosinophils in PC niches showed a high proliferation rate argues against this option (Fig. 4B and C). A variety of other hematopoietic accessory cell types has been described [11, 17–19, 27], but we have not detected any long-lived hematopoietic cells in the vicinity of memory PCs.

Moreover, here we show that PCs can survive for short times without the continued presence of radiation-sensitive eosinophils, when these are killed by irradiation. Two recent studies have investigated the repopulation of the hematopoietic compartment after irradiation in situ [28, 29]. However, our study is the first one to focus on the repopulation of the PC niche, showing that PCs and stroma cells are the only niche components surviving the irradiation (Fig. 5C). Apparently, the PCs can survive until the niche is repopulated by eosinophils, a timespan not exactly determined so far. In this phase, stromal cells supposedly are the sole supporters of PC survival.

In order to further understand the biology of the PC niches it will be crucial to elucidate the mechanisms of how the stromal cells regulate PC survival. The static interaction between PCs and stromal cells is likely mediated by a combination of the adhesion molecules VLA-4 and LFA-1, as blocking their interactions by administration of blocking antibodies in vivo results in a loss of BM PCs [10]. Our data suggest that the PC niches may provide attraction for eosinophils after irradiation. It is currently unclear which signals attract accessory cells to the niches. One possibility is that stromal cells attract them via the CXCL12-CXCR4 axis. Eosinophils have been shown to express CXCR4 [15, 30]. Activation of eosinophils in the course of an immunization has recently been shown to enhance their production of PC survival factors [31]. Another option is that PCs, once they are sessile, are instructed to produce chemoattractants for accessory niche cells themselves. Both options are possible and cannot be discriminated so far.

The number of plasmablasts initially entering the BM after an immunization rapidly decreases [7], most likely because plasmablasts which do not reach a survival niche and dock onto a stromal cell either die in situ or leave the BM. Confirming previous analyses, where BrdU incorporation was used [2], we did not detect proliferative activity in resident BM PCs.

Our finding that the stromal cells forming PC survival niches do not proliferate after immunization indicates that their numbers are fixed. Therefore, they might be the controlling elements for the homeostasis of the long-lived PC compartment and are likely candidates for the principal organizers of the PC survival niche.

Materials and methods

Mice

Blimp-1:GFP [32], Del-Cre x ROSA-tdRFP (tdRFP mice) [33, 34], Ubq:GFP [35], mAG-hGeminin [23] mice were bred and maintained under SPF conditions at the "Bundesinstitut fuer Risikobewertung" (BfR, Berlin, Germany). C57BL6/J mice (Charles River) were maintained at the DRFZ. All experiments were performed according to institutional guidelines and German Federal laws on animal protection (LaGeSo Berlin). Mice were immunized with 100 μg 4-hydroxy-3-nitrophenylacetyl hapten-coupled chicken gamma globulin (NP-CGG) (Rockland) in aluminium hydroxide (Imject Alum, ThermoScientific), 21 days later mice were challenged again with 50 μg soluble NP-CGG intravenously (i.v.) or twice with 50 μg alum-precipitated NP-CGG intraperitoneally (i.p.) at an interval of 21 days. Mice were analyzed at day 12 or day 30 after secondary (i.v.) or tertiary (i.p.) immunization. Total and antigen-specific PC numbers in the chimeras were comparable to immunized Blimp-1 reporter mice (Supporting Information Fig. 3). BM chimeras were generated from tdRFP or Ubq:GFP mice. The mice were irradiated twice (within 3 h) with 3.8 Gray (Gy) and reconstituted 24 h later with 3×10^6 total BM cells (Blimp-1:GFP or C57BL/6J), immunomagnetically depleted for $CD90^+$ cells (Microbeads, Miltenyi Biotec). Mice were treated with 1 mg/mL neomycin (Sigma) and vitamins (Ursovit, Serumwerke Bernburg) for 16 days,

starting 2 days before irradiation. Four weeks after reconstitution, mice were immunized as indicated above.

Antibodies and reagents

The following antibodies and reagents were used for cytometry: anti-kappa light chain-FITC (clone 187.1, DRFZ), CGG-digoxigenin (Rockland, DRFZ) with anti-digoxigenin-Alexa Fluor 405 (DRFZ), anti-CD45-PerCP-Cy5.5 (clone 30F11, EBioscience), anti-CD11b-Pacific Blue (clone M1/70.15.11, DRFZ), anti-Siglec-F-biotin (goat polyclonal, R&D) with Streptavidin-PerCP-eFluor710 (EBioscience), anti-Ly6G/C(Gr-1)-FITC (clone RB6–8C5, DRFZ). Antibodies for histology: anti-mouse-MBP (clone MT-14.7, laboratory of J. and N. Lee, Mayo Clinic, Scottsdale, Arizona), anti-mouse-CD45R(B220)-Alexa Fluor 594 (RA3.6B2, DRFZ), anti-laminin (polyclonal rabbit, Sigma) anti-mouse-lambda1 light chain and kappa light chain-FITC and -Cy5 (clones LS136 and 187.1, DRFZ), anti-mouse-CD106 (VCAM-1)-biotin (clone 429, EBioscience), anti-collagen IV (polyclonal goat, Millipore), anti-human-fibronectin (polyclonal rabbit, Sigma), anti-mouse-osteocalcin (polyclonal rabbit, Enzo), anti-mouse-CD105 (clone MJ7/18, EBioscience), anti-GFP-Alexa Fluor 488 (polyclonal goat, Rockland, DRFZ), anti-mouse-CD3 (clone EBio500A2, EBioscience), anti-mouse-CD4 (clone GK1.5, DRFZ), CGG-digoxigenin (Rockland, DRFZ), anti-RFP-biotin (polyclonal rabbit, Rockland), anti-mouse-CD45 (clone 30F11, EBioscience), anti-mouse-CD41 (clone MWReg30, BD). Secondary reagents used are as follows: anti-rat IgG-Alexa Fluor 488/555/594/647 (Invitrogen), anti-rabbit IgG-Alexa Fluor 555/647 (Invitrogen), anti-goat IgG-Alexa Fluor 555 (Invitrogen), anti-hamster IgG-Alexa Fluor 594 (Invitrogen), Streptavidin-Alexa Fluor 555/647 (Invitrogen), anti-digoxigenin-Alexa Fluor 405 Fab-fragments (Roche, DRFZ).

In vivo EdU pulse-chase method

Mice were fed with 1.25 mg 5-ethynyl-2′-deoxyuridine (EdU)/mouse/day (Invitrogen) in agarose-gel pads with glucose for 12 days, starting with the day of the last immunization. Some mice were analyzed after 12 days of EdU-feeding (pulse cohort), others were analyzed after a chase period of 18 days (without EdU, chase cohort).

Preparation of bone marrow histological sections and confocal microscopy

Femurs were fixed in 4% paraformaldehyde, equilibrated in 30% sucrose/PBS (Merck). Bones were frozen and cryosectioned using Kawamoto's film method [36]. Sections of 7 μm were stained with antibodies in 5% FCS/PBS/0.1% Tween after blocking with 5% FCS/PBS for 30 min. EdU-staining of BM sections was performed using Click-iT™ EdU Imaging Kits (Invitrogen). Sections were stained with 1 μg/mL DAPI (Sigma) in PBS and mounted with fluorescent mounting medium (DAKO). If not stated otherwise, confocal images were generated using a 20×/0.5 numerical aperture (NA) air objective lens on a Zeiss LSM710, equipped with Zen 2010 Version 6.0 software. Overview images of complete femoral BM sections were generated by three-dimensional tile scanning with a 20×/0.5 NA air objective lens. The displayed overview image is comprised of three separate tile scans, with 18–21 maximum intensity projections of z-stacks (tiles) each with 1.3 μm z-resolution and x-y resolution of 1024 × 1024 pixels. Tiles were recorded with an overlap of 10% and projections stitched by the acquisition software to generate three high-resolution images that were then assembled in Photoshop CS4 (Adobe) to form one image of a complete femoral section. Images were analyzed using Zen 2009 Light Edition software (Carl Zeiss MicroImaging).

Automated image analysis

When indicated, histological data was analyzed by an automated image analysis performed by Wimasis Image Analysis (Munich). Cell detection in all color channels was performed using an improved version of the original Otsu algorithm [37]. Cell cluster division was performed by detecting nuclei in the DAPI channel and separating them using an algorithm based on k-means clustering of the intensity levels. Contacts between two cells were defined as overlap of at least one pixel. For the vicinity analysis the cell radius was calculated as any pixel surrounding the cell whose Euclidean distance to the cell's boundary is equal or less than the input distance value (converted from μm to pixels using a scale factor, see supplementary Supporting Information Fig. 10). Cells were counted as neighboring if at least one of their pixels was detected within the vicinity radius.

Manual image analysis

When indicated, contacts between BM cells were counted manually. For manual vicinity analysis, a circle with a defined radius was drawn around the PC, measured from the cell's boundaries. Cells were counted as neighboring cells if they were overlapping with the defined vicinity area.

Simulation of bone marrow histology images with random distribution of hematopoietic cells

A simulation software was written in the C# programming language using Microsoft Visual Studio 2008. The simulation was based on a model of random cell positioning. For each hematopoietic cell population in the simulation (PCs, eosinophils, megakaryocytes or B cells), the total cell number and cell size distribution were matched to the original "real" image identified in the automated image analysis. For each observed image that we wanted to simulate, we ran the model 1000 times and then

analyzed the resulting 1000 simulated images. The resulting simulated cells were saved in .csv text files, and were analyzed by our software to receive the same parameters as provided for the experimentally observed images automatically analyzed by Wimasis. These included the number of cells contacting a cell, the number of cells within a certain radius of a cell, and the number of overlapping pixels between various cell pairs. The results for every "real" image were compared with the average contact counts and vicinity counts of 1000 simulated images (Supporting Information Fig. 4B and 4C).

Workflow for simulations of random cell positioning:

(i) Load the image of the marrow stromal cells into the software.
(ii) Automatically identify the corresponding DAPI image based on file naming conventions. The DAPI image shows the nuclei of all cells in the marrow.
(iii) Use the DAPI image to create a mask that identifies the location of the BM: first, the DAPI image was pixel-dilated in five steps in order to fill in the small holes, then a five-step erosion followed that compensated for the shrinkage of the larger nonmarrow areas. Lastly the image was threshold-adjusted with a manually set background value (Supporting Information Fig. 4A).
(iv) Threshold the stromal cell image with the Otsu method in order to identify the pixels that belong to the stromal cells. These pixels will be used to calculate the overlap and neighborhood density values between the hematopoietic cell types (B cells, eosinophils, and PCs, alternatively megakaryocytes, and PCs) and the stroma.
(v) Automatically load the image segmentation data file for the current image (automated analysis produced by Wimasis; data file identified based on naming convention), and calculate the observed number of B cells, eosinophils, and PCs (or PCs and megakaryocytes). Calculate also the average number of pixels for each cell type, as well as the average cell diameter assuming a circular shape.
(vi) Generate simulated cells randomly and place them on the stromal cell image:
    (a) A linear random number generator was used to determine the type of the newly generated cell (B cell, eosinophil, megakaryocyte or PC).
    (b) A Gaussian random number generator that used the calculated average diameter of the corresponding cell type as the peak value of the Gaussian distribution provided the diameter of the model cell. The width of the Gaussian was determined based on the visual similarity of the measured and simulated images.
    (c) A linear random number generator determined the location of the newly created model cell. Cells were not allowed to overlap the nonmarrow part of the stromal cell image (the DAPI image-based mask was used here to determine the location of the nonmarrow pixels).
    (d) Cells were placed on the stromal image if they did not lie within a predetermined radius of another existing simulated cell. If the newly simulated cell was within an exclusion zone, the location coordinates were thrown away, and new pair of X, Y coordinates were generated randomly, until the new cell was outside the exclusion zones of all existing simulated cells.

Steps vi a–d were repeated until the number of simulated cells reached the experimentally observed number of B cells, eosinophils, and PCs (or megakaryocytes and PCs). The resulting simulated cells were saved in .csv text files, and were analyzed by our software to receive the same parameters as provided for the experimentally observed images automatically analyzed by Wimasis.

Cell preparation and flow cytometry

BM single cell suspensions were prepared from long bones of individual mice. Long bones were opened and flushed with 0.5% BSA/2 mM EDTA/PBS solution. Single cells were collected and erythrocytes lysed using ACK buffer. To prepare single cell suspensions also containing stromal cells, BM was incubated in digestion mix (collagenase type IV (Sigma), Dispase II (Roche Applied Science), and DNAse I (Sigma)). For staining, cells were preincubated in a 0.5% BSA/2 mM EDTA/PBS solution of 20 μg/mL anti-FcgRII/III (2.4G2) (DRFZ) for 10 min on ice. The cells were then stained with antibodies to surface antigens and Fixable Viability Dye eFluor® 780 (EBioscience) for live- and dead-cell population discrimination. For intracellular staining, cells were fixed with 2% PFA and permeabilized with 0.5% Saponin (Sigma) in 0.5% BSA/2 mM EDTA/PBS. EdU staining was performed using Click-iT™ EdU Imaging/Flow Cytometry Kits (Invitrogen). Stained samples were analyzed in a BD LSRFortessa cytometer (BD Biosciences) or MACSQuant analyzer (Miltenyi Biotec). Flow cytometric data were analyzed with FlowJo (Tree Star, Inc.) software. For calculation of total BM PC numbers, the cell number of all viable nucleated cells from two tibiae for each individual animal was multiplied with a correction factor of 14.49 [38].

Statistical analysis

Statistical analysis was performed with GraphPad Prism 6 software, as indicated in figure legends. Unless otherwise indicated, all values indicate median percentages with range in parentheses. p values ≤ 0.05 are considered significant differences. Asterisks in figures indicate the following p values: ns: $p > 0.05$; *: $p \leq 0.05$; **: $p \leq 0.01$; ***: $p \leq 0.001$; ****: $p \leq 0.0001$.

Intravital multiphoton imaging

Intravital imaging was performed 24 h after an adoptive transfer of plasmablasts from spleen and BM, which were FACS-sorted from Blimp1:GFP mice at day 5 after boost based on staining

with CD138-PE (BD, clone 281–2) and subsequently labeled with CellTracker Orange, into mice with green fluorescent stroma. The surgical preparation of the tibia for intravital microscopy was performed as previously described [39]. Imaging was performed with a two-photon laser-scanning microscope (TriMScope, LaVision BioTec, Bielefeld, Germany) equipped with a 20×/0.95 NA objective lens (Olympus, Hamburg, Germany) and a tuneable femtosecond-pulsed Ti:Sa laser (140 fs, 80 MHz, Chameleon Ultra II, Coherent, Germany). Stacks of 24 optical sections (x: 300 μm, y: 300 μm, z: 3 μm) were acquired every 30 s at 850 nm. Emitted light was detected with photomultiplier tubes after having passed through 460/60, 525/50, and 593/40 nm bandpass filters. Volocity software (Perkin Elmer) was used to create sequences of image stacks.

Acknowledgments: We thank Sabine Gruczek, Patrick Thiemann, and Manuela Ohde for assistance with animal care. We thank Toralf Kaiser, Jenny Kirsch, Tuula Geske, Heidi Schliemann and Heidi Hecker-Kia, Robert Günther and Hilmar Frank for excellent technical assistance and M. McGrath, K. Tokoyoda, H. Radbruch, F. Hiepe, B. Hoyer, C. Berek, T. Chu, T. Dörner for discussions. We thank J. and N. Lee, Mayo Clinic, Scottsdale, Arizona, USA for MBP-specific antibodies, A. Miyawaki, RIKEN Brain Institute, Japan for the mAG-huGeminin cell cycle reporter mice, S. Nutt, WEHI Melbourne, Australia for Blimp-1:GFP reporter mice and H.J. Fehling, Institute of Immunology, University of Ulm, Germany for tdRFP mice. This work was supported by DFG HA5354/4-1, DFG Transregio 130 (project 17) and JIMI-a DFG core facility network grant for intravital microscopy to A.E.H., by the DFG priority program SPP1468 IMMUNOBONE to H.D.C. and to A.R. and the DFG Transregio 130 (project 16), as well as by the European Research Council through an Advanced Grant (ERC-2010-AdG_20100317 Grant 268987) to A.R.. S.Z. was supported by the International Max Planck Research School for Infectious Diseases and Immunology Berlin (IMPRS-IDI).

Conflict of interest: The authors declare no financial or commercial conflict of interest.

References

1 **Tokoyoda, K., Hauser, A. E., Nakayama, T. and Radbruch, A.**, Organization of immunological memory by bone marrow stroma. *Nat. Rev. Immunol.* 2010. **10**: 193–200.

2 **Manz, R. A., Thiel, A. and Radbruch, A.**, Lifetime of plasma cells in the bone marrow. *Nature* 1997. **388**: 133–134.

3 **Tokoyoda, K., Zehentmeier, S., Hegazy, A. N., Albrecht, I., Grun, J. R., Lohning, M. and Radbruch, A.**, Professional memory CD4+ T lymphocytes preferentially reside and rest in the bone marrow. *Immunity* 2009. **30**: 721–730.

4 **Radbruch, A., Muehlinghaus, G., Luger, E. O., Inamine, A., Smith, K. G., Dorner, T. and Hiepe, F.**, Competence and competition: the challenge of becoming a long-lived plasma cell. *Nat. Rev. Immunol.* 2006. **6**: 741–750.

5 **Tokoyoda, K., Zehentmeier, S., Chang, H. D. and Radbruch, A.**, Organization and maintenance of immunological memory by stroma niches. *Eur. J. Immunol.* 2009. **39**: 2095–2099.

6 **Tokoyoda, K., Egawa, T., Sugiyama, T., Choi, B. I. and Nagasawa, T.**, Cellular niches controlling B lymphocyte behavior within bone marrow during development. *Immunity* 2004. **20**: 707–718.

7 **Hauser, A. E., Debes, G. F., Arce, S., Cassese, G., Hamann, A., Radbruch, A. and Manz, R. A.**, Chemotactic responsiveness toward ligands for CXCR3 and CXCR4 is regulated on plasma blasts during the time course of a memory immune response. *J. Immunol.* 2002. **169**: 1277–1282.

8 **Hargreaves, D. C., Hyman, P. L., Lu, T. T., Ngo, V. N., Bidgol, A., Suzuki, G., Zou, Y. R. et al.**, A coordinated change in chemokine responsiveness guides plasma cell movements. *J. Exp. Med.* 2001. **194**: 45–56.

9 **Cassese, G., Arce, S., Hauser, A. E., Lehnert, K., Moewes, B., Mostarac, M., Muehlinghaus, G. et al.**, Plasma cell survival is mediated by synergistic effects of cytokines and adhesion-dependent signals. *J. Immunol.* 2003. **171**: 1684–1690.

10 **DiLillo, D. J., Hamaguchi, Y., Ueda, Y., Yang, K., Uchida, J., Haas, K. M., Kelsoe, G. et al.**, Maintenance of long-lived plasma cells and serological memory despite mature and memory B cell depletion during CD20 immunotherapy in mice. *J. Immunol.* 2008. **180**: 361–371.

11 **Winter, O., Moser, K., Mohr, E., Zotos, D., Kaminski, H., Szyska, M., Roth, K. et al.**, Megakaryocytes constitute a functional component of a plasma cell niche in the bone marrow. *Blood* 2010. **116**: 1867–1875.

12 **Belnoue, E., Pihlgren, M., McGaha, T. L., Tougne, C., Rochat, A. F., Bossen, C., Schneider, P. et al.**, APRIL is critical for plasmablast survival in the bone marrow and poorly expressed by early life bone marrow stromal cells. *Blood* 2008. **111**: 2755–2764.

13 **Benson, M. J., Dillon, S. R., Castigli, E., Geha, R. S., Xu, S., Lam, K. P. and Noelle, R. J.**, Cutting Edge: The Dependence of Plasma Cells and Independence of Memory B Cells on BAFF and APRIL. *J. Immunol.* 2008. **180**: 3655–3659.

14 **Peperzak, V., Vikstrom, I., Walker, J., Glaser, S. P., LePage, M., Coquery, C. M., Erickson, L. D. et al.**, Mcl-1 is essential for the survival of plasma cells. *Nat. Immunol.* 2013. **14**: 290–297.

15 **Chu, V. T., Frohlich, A., Steinhauser, G., Scheel, T., Roch, T., Fillatreau, S., Lee, J. J. et al.**, Eosinophils are required for the maintenance of plasma cells in the bone marrow. *Nat. Immunol.* 2011. **12**: 151–159.

16 **Ohnmacht, C., Pullner, A., van Rooijen, N. and Voehringer, D.**, Analysis of eosinophil turnover in vivo reveals their active recruitment to and prolonged survival in the peritoneal cavity. *J. Immunol.* 2007. **179**: 4766–4774.

17 **Rozanski, C. H., Arens, R., Carlson, L. M., Nair, J., Boise, L. H., Chanan-Khan, A. A., Schoenberger, S. P. et al.**, Sustained antibody responses depend on CD28 function in bone marrow-resident plasma cells. *J. Exp. Med.* 2011. **208**: 1435–1446.

18 **Rodriguez Gomez, M., Talke, Y., Goebel, N., Hermann, F., Reich, B. and Mack, M.**, Basophils support the survival of plasma cells in mice. *J. Immunol.* 2010. **185**: 7180–7185.

19 **Belnoue, E., Tougne, C., Rochat, A. F., Lambert, P. H., Pinschewer, D. D. and Siegrist, C. A.**, Homing and adhesion patterns determine the cellular composition of the bone marrow plasma cell niche. *J. Immunol.* 2012. **188**: 1283–1291.

20 **Fooksman, D. R., Schwickert, T. A., Victora, G. D., Dustin, M. L., Nussenzweig, M. C. and Skokos, D.**, Development and migration of plasma cells in the mouse lymph node. *Immunity* 2010. **33**: 118–127.

21 **Amanna, I. J., Carlson, N. E. and Slifka, M. K.**, Duration of humoral immunity to common viral and vaccine antigens. *N. Engl. J. Med.* 2007. **357**: 1903–1915.

22 **Manz, R. A., Lohning, M., Cassese, G., Thiel, A. and Radbruch, A.**, Survival of long-lived plasma cells is independent of antigen. *Int. Immunol.* 1998. **10**: 1703–1711.

23 **Sakaue-Sawano, A., Kurokawa, H., Morimura, T., Hanyu, A., Hama, H., Osawa, H., Kashiwagi, S. et al.**, Visualizing spatiotemporal dynamics of multicellular cell-cycle progression. *Cell* 2008. **132**: 487–498.

24 **Sapoznikov, A., Pewzner-Jung, Y., Kalchenko, V., Krauthgamer, R., Shachar, I. and Jung, S.**, Perivascular clusters of dendritic cells provide critical survival signals to B cells in bone marrow niches. *Nat. Immunol.* 2008. **9**: 388–395.

25 **Pereira, J. P., An, J., Xu, Y., Huang, Y. and Cyster, J. G.**, Cannabinoid receptor 2 mediates the retention of immature B cells in bone marrow sinusoids. *Nat. Immunol.* 2009. **10**: 403–411.

26 **Omatsu, Y., Sugiyama, T., Kohara, H., Kondoh, G., Fujii, N., Kohno, K. and Nagasawa, T.**, The essential functions of adipo-osteogenic progenitors as the hematopoietic stem and progenitor cell niche. *Immunity* 2010. **33**: 387–399.

27 **Matthes, T., Dunand-Sauthier, I., Santiago-Raber, M. L., Krause, K. H., Donze, O., Passweg, J., McKee, T. et al.**, Production of the plasma-cell survival factor a proliferation-inducing ligand (APRIL) peaks in myeloid precursor cells from human bone marrow. *Blood* 2011. **118**: 1838–1844.

28 **Takaku, T., Malide, D., Chen, J., Calado, R. T., Kajigaya, S. and Young, N. S.**, Hematopoiesis in 3 dimensions: human and murine bone marrow architecture visualized by confocal microscopy. *Blood* 2010. **116**: 4175–4184.

29 **Malide, D., Metais, J. Y. and Dunbar, C. E.**, Dynamic clonal analysis of murine hematopoietic stem and progenitor cells marked by 5 fluorescent proteins using confocal and multiphoton microscopy. *Blood* 2012. **120**: e105–116.

30 **Nagase, H., Miyamasu, M., Yamaguchi, M., Fujisawa, T., Ohta, K., Yamamoto, K., Morita, Y. et al.**, Expression of CXCR4 in eosinophils: functional analyses and cytokine-mediated regulation. *J. Immunol.* 2000. **164**: 5935–5943.

31 **Chu, V. T. and Berek, C.**, Immunization induces activation of bone marrow eosinophils required for plasma cell survival. *Eur. J. Immunol.* 2012. **42**: 130–137.

32 **Kallies, A., Hasbold, J., Tarlinton, D. M., Dietrich, W., Corcoran, L. M., Hodgkin, P. D. and Nutt, S. L.**, Plasma cell ontogeny defined by quantitative changes in blimp-1 expression. *J. Exp. Med.* 2004. **200**: 967–977.

33 **Luche, H., Weber, O., Nageswara Rao, T., Blum, C. and Fehling, H. J.**, Faithful activation of an extra-bright red fluorescent protein in "knock-in" Cre-reporter mice ideally suited for lineage tracing studies. *Eur. J. Immunol.* 2007. **37**: 43–53.

34 **Schwenk, F., Baron, U. and Rajewsky, K.**, A cre-transgenic mouse strain for the ubiquitous deletion of loxP-flanked gene segments including deletion in germ cells. *Nucleic Acids Res.* 1995. **23**: 5080–5081.

35 **Schaefer, B. C., Schaefer, M. L., Kappler, J. W., Marrack, P. and Kedl, R. M.**, Observation of antigen-dependent CD8+ T-cell/ dendritic cell interactions in vivo. *Cell Immunol.* 2001. **214**: 110–122.

36 **Kawamoto, T.**, Use of a new adhesive film for the preparation of multi-purpose fresh-frozen sections from hard tissues, whole-animals, insects and plants. *Arch. Histol. Cytol.* 2003. **66**: 123–143.

37 **Otsu, N.**, A threshold selection method from gray-level histograms. *IEEE Trans. Sys. Man. Cyber.* 1979. **9**: 62–66.

38 **Chervenick, P. A., Boggs, D. R., Marsh, J. C., Cartwright, G. E. and Wintrobe, M. M.**, Quantitative studies of blood and bone marrow neutrophils in normal mice. *Am. J. Physiol.* 1968. **215**: 353–360.

39 **Kohler, A., De Filippo, K., Hasenberg, M., van den Brandt, C., Nye, E., Hosking, M. P., Lane, T. E. et al.**, G-CSF-mediated thrombopoietin release triggers neutrophil motility and mobilization from bone marrow via induction of Cxcr2 ligands. *Blood* 2011. **117**: 4349–4357.

Abbreviations: **APRIL**: a proliferation-inducing ligand · **BM**: bone marrow · **CGG**: chicken gamma globulin · **EdU**: 5-ethynyl-2′-deoxyuridine · **Gy**: gray · **MBP**: major basic protein · **NA**: numerical aperture · **NP**: 4-hydroxy-3-nitrophenylacetyl hapten · **NP-CGG**: NP coupled to CGG · **PC**: plasma cell · **RFP**: red fluorescent protein

Full correspondence: Dr. Anja Erika Hauser, Deutsches Rheuma-Forschungszentrum (DRFZ), Charitéplatz 1, D-10117 Berlin, Germany
Fax: +49-30-28460-603
e-mail: hauser@drfz.de

See accompanying Commentary: http://dx.doi.org/10.1002/eji.201444871

Received: 19/11/2013
Revised: 14/3/2014
Accepted: 23/4/2014
Accepted article online: 28/4/2014

